LETTER

doi:10.1038/nature19113

Key new pieces of the HIMU puzzle from olivines and diamond inclusions

Yaakov Weiss[1], Cornelia Class[1], Steven L. Goldstein[1,2] & Takeshi Hanyu[3]

Mantle melting, which leads to the formation of oceanic and continental crust, together with crust recycling through plate tectonics, are the primary processes that drive the chemical differentiation of the silicate Earth. The present-day mantle, as sampled by oceanic basalts, shows large chemical and isotopic variability bounded by a few end-member compositions[1]. Among these, the HIMU end-member (having a high U/Pb ratio, μ) has been generally considered to represent subducted/recycled basaltic oceanic crust[2–5]. However, this concept has been challenged by recent studies of the mantle source of HIMU magmas. For example, analyses of olivine phenocrysts in HIMU lavas indicate derivation from the partial melting of peridotite, rather than from the pyroxenitic remnants of recycled oceanic basalt[6]. Here we report data that elucidate the source of these lavas: high-precision trace-element analyses of olivine phenocrysts point to peridotite that has been metasomatized by carbonatite fluids. Moreover, similarities in the trace-element patterns of carbonatitic melt inclusions in diamonds[7] and HIMU lavas indicate that the metasomatism occurred in the subcontinental lithospheric mantle, fused to the base of the continental crust and isolated from mantle convection. Taking into account evidence from sulfur isotope data[8] for Archean to early Proterozoic surface material in the deep HIMU mantle source, a multi-stage evolution is revealed for the HIMU end-member, spanning more than half of Earth's history. Before entrainment in the convecting mantle, storage in a boundary layer, upwelling as a mantle plume and partial melting to become ocean island basalt, the HIMU source formed as Archean–early Proterozoic subduction-related carbonatite-metasomatized subcontinental lithospheric mantle.

The spectrum of chemical compositions in oceanic basalts reflects the large-scale chemical heterogeneity of Earth's mantle, with end-members ranging from the trace-element-depleted upper-mantle source of mid-ocean ridge basalts (MORBs), often called 'depleted MORB mantle', to three distinct trace-element 'enriched mantle flavours'[4] in ocean island basalts (OIBs) known as EM1, EM2 and HIMU[1] (Extended Data Fig. 1). Among these end-members, HIMU basalts stand out with the highest Pb isotope ratios, high Os isotope ratios, low Sr isotope ratios that are slightly higher than those of depleted MORB, and Nd–Sr isotope ratios that plot below the so-called Nd–Sr mantle array[1,2,9]. Their mantle source has generally been considered to represent recycled basaltic oceanic crust that preferentially lost fluid-mobile trace elements, such as the alkali metals and Pb, during hydrothermal alteration at ocean ridges or through slab dehydration processes during subduction[2–5]. Sulfur isotopes in HIMU basalts show mass-independent fractionation generated by ultraviolet radiation in the Archean to early Proterozoic Earth's oxygen-poor atmosphere[8], thus indicating the presence of recycled Archean to early Proterozoic surface material in the HIMU mantle source. However, critical observations challenge the view that HIMU represents subducted basaltic oceanic crust. For example, Pb isotopes in MORB do not trend towards HIMU values (Extended Data Fig. 1), so HIMU is not a mixing end-member of most MORBs[4,10]. In addition, recycled basalt transforms to garnet- and clinopyroxene-rich and olivine-poor (pyroxenitic) mantle lithologies under mantle conditions, but minor and trace elements in olivine phenocrysts found in HIMU basalts indicate melt sources that are controlled by olivine-dominated (peridotitic) mantle rocks[6]. The nature of the HIMU mantle source therefore remains a puzzle.

We report high-precision trace-element data on olivine phenocrysts in HIMU lavas from Mangaia and Tubuai in the Cook–Austral Islands, South Pacific[5], and in lavas from Karthala, Grande Comore Island, in the Indian Ocean[11] (see Supplementary Data 1), which show intermediate Nd–Sr–Pb isotope ratios between the HIMU and EM1 mantle end-members. Mangaia–Tubuai–Karthala (MTK) olivines have lower Mg/Fe ratios than do primitive MORBs ($Fo_{88–77}$ versus Fo_{92}, respectively; where Fo# = 100Mg/(Mg + Fe) (the molar ratio) in olivine, which decreases as magmas undergo crystallization (Fig. 1a)). Comparing olivines with similar Fo#, Ni abundances in MTK olivines are lower than Koolau (in Hawaii, from a mantle source with substantial pyroxenite) and higher than MORB (from melting of mainly peridotite)[12]. Nickel abundances have been used to evaluate mantle source lithologies because Ni fits into the lattice structure of olivine and thus tends to remain in olivine during melting. Magmas derived from the partial melting of olivine-rich rocks such as peridotite are therefore expected to have lower Ni abundances than those derived from olivine-poor rocks such as pyroxenite[12]. Possible explanations for the higher Ni concentrations observed in MTK olivines compared with MORB, on the basis of the source lithology, include greater contributions from pyroxenite sources[12] and the mixing of parental and evolved peridotite-sourced melts in a shallow magma chamber[6]. Alternatively, Ni variability can depend on the melting conditions[13], because its partitioning varies with the melting depth (temperature). Melting of OIBs at higher temperatures and greater depths than MORBs would yield magmas with higher Ni contents, and therefore the effect of temperature must be taken into account in interpreting Ni abundances. If we assume that MORB segregates at shallow depths beneath ocean ridges, and that MTK magmas segregate near the base of the old oceanic lithosphere with a pressure difference of around 1–2 GPa (approximately 35–70 km depth), this could result in a difference in the Ni content of 300–500 parts per million (p.p.m.) (details in the legend of Extended Data Fig. 2). When corrected for the depth of magma segregation, MTK olivines fit a modelled olivine liquid line of descent for Mangaia primary magma[6] and fall on the crystallization trend of MORB phenocrysts (Extended Data Fig. 2). Although the Ni contents and Ni/Mg ratios in olivine phenocrysts probably reflect melting conditions as well as source compositions, the data clearly indicate a dominant role for peridotite lithologies in the HIMU source.

The Mn/Fe ratio in olivine phenocrysts is a more robust source lithology discriminator than Ni, as Mn/Fe variability is essentially

[1]Lamont-Doherty Earth Observatory of Columbia University, Palisades, New York 10964, USA. [2]Department of Earth and Environmental Sciences, Columbia University, Palisades, New York 10964, USA. [3]Department of Solid Earth Geochemistry, Japan Agency for Marine-Earth Science and Technology, Yokosuka 237-0061, Japan.

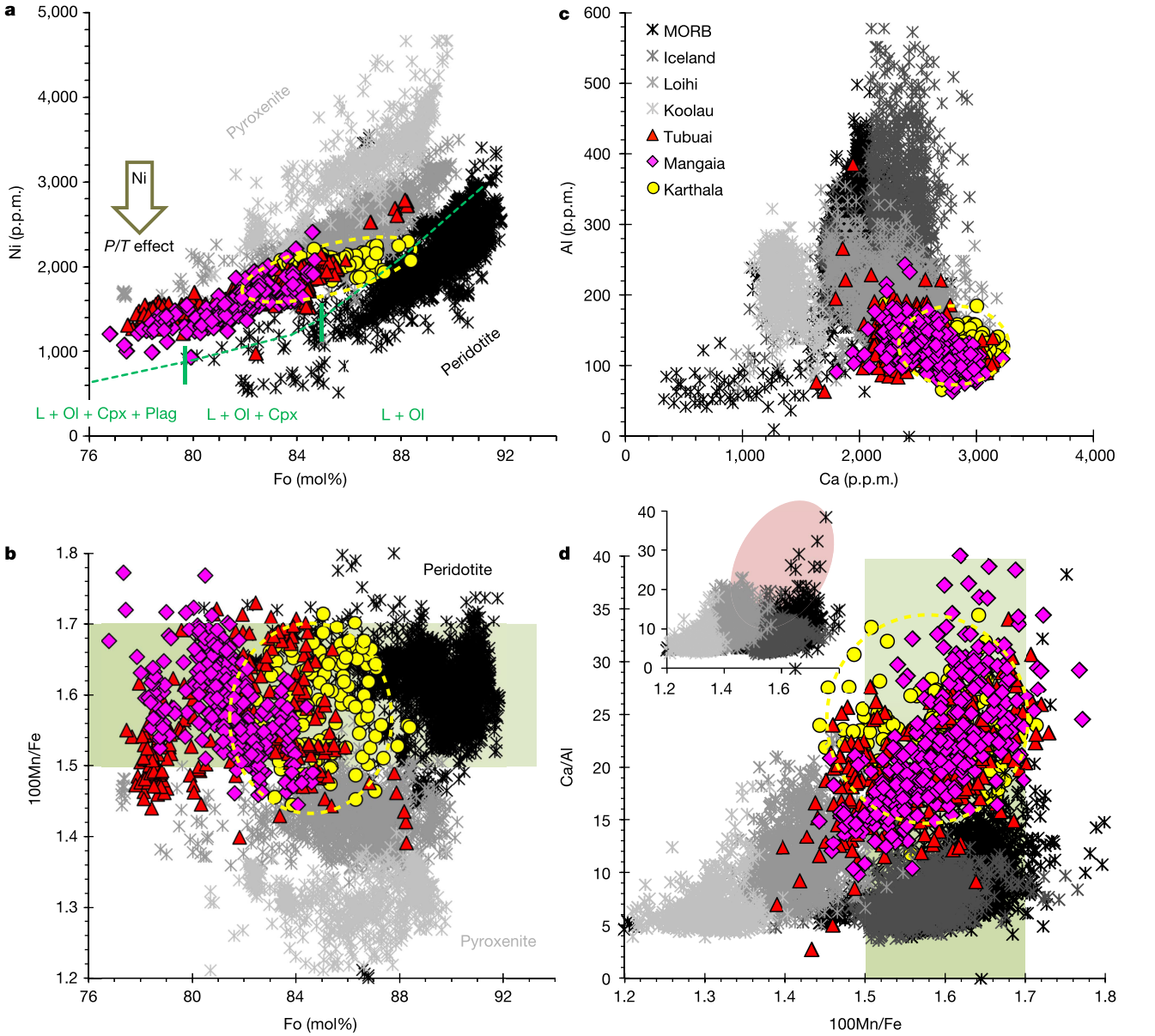

Figure 1 | Compositions of olivine phenocrysts from HIMU (Mangaia, Tubuai) and intermediate HIMU–EM1 (Karthala) lavas. a, Fo versus Ni. The green dashed line is the calculated olivine liquid line of descent for Mangaia primary magma[6]; green vertical lines separate the intervals with L, liquid; Ol, olivine; Cpx, clinopyroxene; Plag, plagioclase. The arrow pointing to lower Ni indicates the effect of increasing pressure and/or temperature ('*P*/*T* effect') on Ni in olivine (additional details are in the legend of Extended Data Fig. 2). **b**, Fo versus 100Mn/Fe; the green shading emphasizes the similarity in the 100Mn/Fe ratios between MORB and HIMU olivines as opposed to pyroxenitic source lithologies. **c**, Ca versus Al (p.p.m.). **d**, 100Mn/Fe versus Ca/Al; the green shading has the same function as in **b**. The inset in **d** highlights the enrichment of Ca and depletion of Al in olivines in HIMU lavas (rose shading) compared with non-HIMU basalts. The yellow ellipses encompass >95% of the data points for Karthala olivine. Iceland data in **a** and **b** overlap with MORB and are not shown for clarity. Data for Mangaia, Tubuai and Karthala olivines are provided in Supplementary Data 1; data for MORB, Iceland and Hawaiian lavas are from ref. 12.

independent of Fo content and differences in the temperatures of melting and crystallization. Rather, Mn/Fe is strongly dependent on the olivine/garnet ratio and the modal abundance of garnet in the magma source; and peridotite (high-olivine) sources produce magmas with higher Mn/Fe[14]. For MTK olivines, 100Mn/Fe is 1.5–1.7, similar to MORB phenocrysts for which peridotitic sources have been inferred and higher than those for which pyroxenite sources have been inferred[12] (Fig. 1b), thus providing further evidence for production of HIMU magmas by peridotite melting.

A key observation from our new data (Fig. 1c) is that HIMU and Karthala olivines are characterized by high Ca (up to 3,200 p.p.m.) and low Al (80–180 p.p.m.) contents, resulting in distinctly high Ca/Al ratios that are far outside the range previously reported for olivines from MORB and OIB lavas (Fig. 1d). Temperature-dependent variations in the Ca and Al contents in olivines in peridotite xenoliths, oceanic basalts and experimental studies of peridotite melting[15–17] indicate that Ca/Al ratios in olivine decrease with increasing temperature (Extended Data Figs 3 and 4). Thus, the elevated Ca/Al ratios in the HIMU olivines, which crystallized from 'hot plume' magmas, compared with olivines with lower Ca/Al contents from 'cooler MORB' (or for that matter, lower Ca/Al ratios in other 'hot OIBs'), cannot be explained by temperature differences. In addition, the Ca/Al ratio in olivines from MORBs, Hawaii–Loihi and Hawaii–Koolau are similar (Fig. 1d), despite differences in the source lithologies (the source of MORB is peridotite-dominated with little or no garnet in the melt residue, Hawaii–Loihi's source is peridotite-dominated with residual garnet and Hawaii–Koolau is pyroxenite-dominated with residual garnet), indicating that the effects of the source mineralogy on

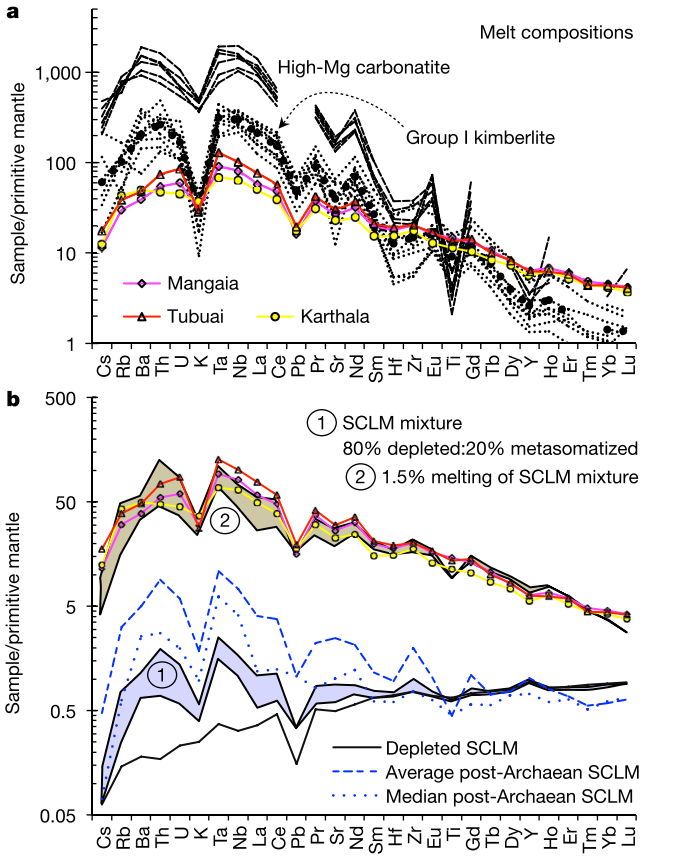

Figure 2 | Normalized trace-element patterns comparing HIMU–EM1 lavas (Mangaia, Tubuai and Karthala), Group I kimberlites, high-Mg carbonatitic fluids from diamond inclusions and the calculated melt of SCLM source compositions. a, The average compositions for Mangaia, Tubuai and Karthala are from the GEOROC database (http://georoc.mpch-mainz.gwdg.de/georoc); Group I kimberlites from Africa, Canada, Siberia, Finland, India and Brazil (thin dotted lines), a global average Group I kimberlite pattern (thick dotted line) and carbonatitic fluids in diamond inclusions (dashed lines) are summarized in ref. 7. **b**, Batch melting of a mixture of 80:20 depleted:metasomatized SCLM peridotite (1) closely reproduces the trace-element pattern of HIMU basalts (2). We used average depleted MORB mantle and average and median post-Archean SCLM compositions to represent depleted and metasomatized rocks, respectively, to derive the mixed SCLM composition and calculated the melt composition (partial melt fraction of 1.5%) for such a source in equilibrium with a modal mineralogy of 72% olivine, 20% orthopyroxene, 2% clinopyroxene, 5% garnet and 1% carbonate. The calculations use partition coefficients for silicate/basaltic melt, except for Pb (which is not controlled by silicates melting and was set to be equal to Ce partitioning values) and carbonate partitioning. Model details are in Supplementary Information (see the trace-element melting model).

Ca/Al ratios are minor. The very high Ca/Al ratio in HIMU and Karthala olivines compared with Hawaii, Iceland and MORB (Fig. 1d) instead reflect the distinct composition of the mantle source of HIMU lavas.

We propose that the exceptionally high Ca/Al ratios in these olivines indicate an enrichment process that involves carbonatitic fluids. Such fluids would have high Ca abundances and low SiO_2 and Al_2O_3 contents, such that on metasomatic interaction with peridotite in the mantle, olivine would not be converted to pyroxene and the lithology would be preserved. A role for carbonatitic metasomatism of the HIMU source is further supported by the presence of carbonate globules in HIMU olivine phenocrysts[18], and high CaO and Ca/Al ratios in HIMU magmas compared with other oceanic basalts[19,20].

The trace-element patterns of HIMU lavas (Fig. 2a) are unique among OIBs[21]. Notably, they are similar to Group I kimberlites[22], which are products of a low degree of partial melting of trace-element-enriched carbonated peridotite. They are also similar to high-Mg carbonatitic melts in diamond fluid inclusions[7], which are direct samples of deep (>150 km) metasomatic fluids in the subcontinental lithospheric mantle (SCLM). All are characterized by enrichment in incompatible elements, but with high Nb and Ta contents compared with La, depletions in the alkali metals (K, Rb, Cs) compared with other highly incompatible elements (Ba, U, Th, La) and depletions in Pb compared with rare earth elements of similar compatibility. These patterns reflect the trace-element enrichment and depletion processes experienced by their mantle sources integrated over geologic time, and thus their distinctive compositional similarities indicate similar histories. There are also differences: the trace element patterns of kimberlites and deep carbonatitic melts are subparallel to HIMU but at higher abundances for most highly incompatible elements (Cs to Sm in Fig. 2a), and they display depletions in Ti, Zr and Hf compared with rare earth elements of similar incompatibility during partial melting. These differences could reflect variables such as source heterogeneity, different elemental partitioning between carbonatite and peridotite versus silicate melts and peridotite, differences in the degree of melting between carbonatite (<0.5% partial melting), kimberlite (<2%) and OIBs (<5%) and the retention of these elements in accessory phases during partial melting. The HIMU trace-element patterns also mimic those of Archean metasomatized mantle xenoliths[23] and average post-Archean SCLM[24] (Fig. 2b), which can be produced by carbonatitic melts interacting with depleted mantle compositions[7]. To test the possible petrogenetic link between HIMU and SCLM sources metasomatized by carbonatitic fluids, we calculated the trace-element patterns of melts from a SCLM source that is composed of both 'normal' (trace-element-depleted) peridotite and metasomatized peridotite (80:20, respectively; see details of the trace-element model in the legend of Fig. 2b and Supplementary Information). The calculated melt trace-element patterns show striking similarities to HIMU basalts, thus supporting a linkage between HIMU lavas and SCLM peridotite sources that are metasomatically enriched by carbonatite fluids such as those observed in diamond inclusions.

A major remaining issue is whether such an origin from carbonatite metasomatized SCLM is consistent with the unique isotopic compositions of HIMU lavas. The Nd–Sr–Pb isotopes in Group I kimberlites and continental carbonatites fall 'below' the Nd–Sr mantle array, lying on the 'LoNd array'[25] between the HIMU and EM1 global mantle end-members (Extended Data Fig. 1). Although this group covers a large range of isotope ratios, it includes the HIMU compositions as an end-member. Thus Nd–Sr–Pb isotopes, like the trace-element patterns (Fig. 2), support a genetic relationship between HIMU lavas and metasomatized carbonated peridotite sources in the SCLM. However, the low Os isotope ratios observed in most SCLM xenolith studies contrast with the high values in HIMU lavas, which has led to conclusions that recycled SCLM is not an important component in HIMU OIB[9,26].

To determine whether the Os isotopes in HIMU lavas preclude an SCLM source, we accessed and revised the mantle xenolith data from cratonic settings (see Supplementary Data 2) in the PetDB database (http://www.earthchem.org/petdb) (formerly the Deep Lithosphere Dataset, http://www.earthchem.org/deeplith). The Al_2O_3 content decreases with increasing Mg number (Mg# = Mg/(Mg + Fe), molar ratio) from lherzolite to harzburgite compositions (Fig. 3a), following an 'SCLM depletion trend' that is consistent with incompatible element depletion by melt extraction, leading to SCLM formation. The most melt-depleted (harzburgitic) xenoliths, however, often show high K_2O, Zr/Hf and La/Sm ratios (Fig. 3b–d), consistent with deep carbonatitic metasomatism by fluids such as those in diamond inclusions[7,27]. Importantly, the metasomatized harzburgitic compositions trend towards elevated Re/Os and Os isotope ratios (Fig. 3e, f)—higher than HIMU values. A model calculation (Supplementary Information;

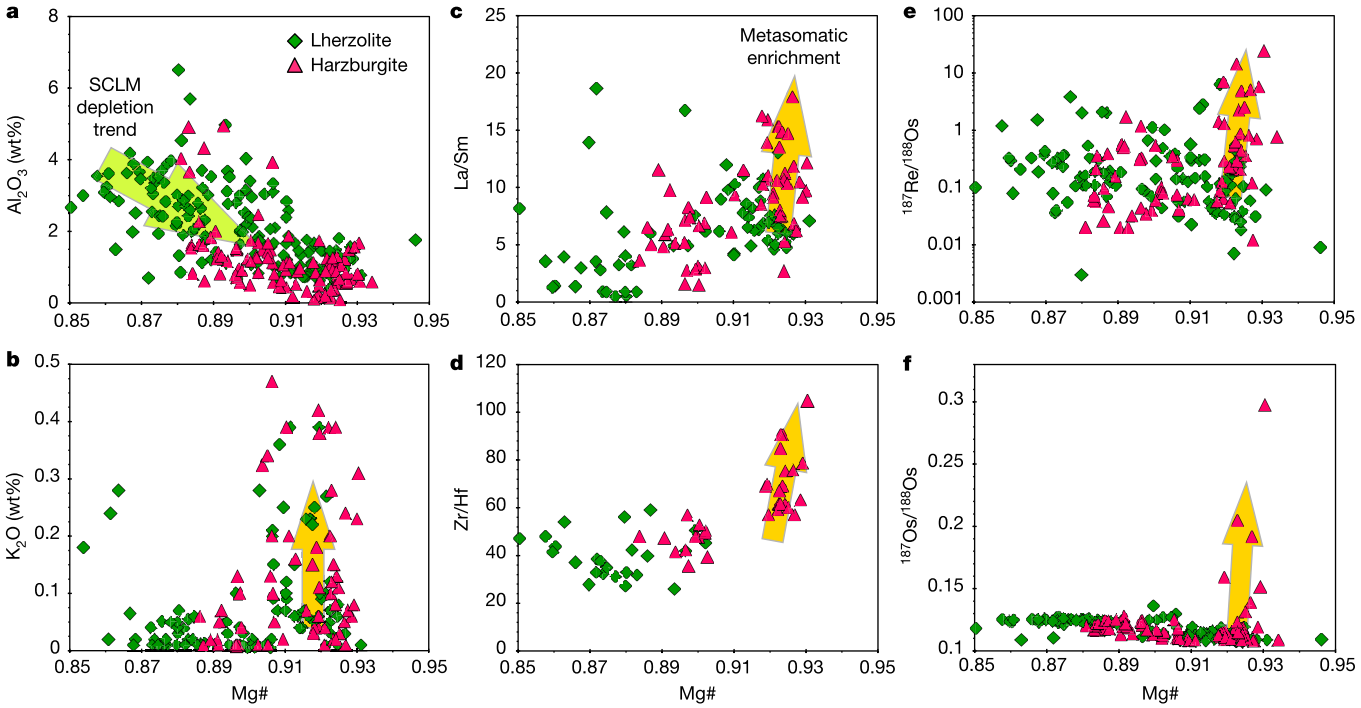

Figure 3 | Mg# versus major element abundances, trace-element ratios, and isotope ratios in cratonic xenoliths. Data are available in Supplementary Data 2. **a**, Al_2O_3. **b**, K_2O. **c**, La/Sm. **d**, Zr/Hf. **e**, $^{187}Re/^{188}Os$. **f**, $^{187}Os/^{188}Os$. The depletion trend of Al_2O_3 (and CaO, not shown) with increasing Mg# (green arrow) reflects the depletion of incompatible elements in the SCLM mantle due to melt extraction. The harzburgite xenoliths show enrichment in K_2O and other incompatible elements, as well as high Zr/Hf ratios due to re-enrichment by metasomatic carbonatitic fluids and melts (orange arrows). Although K_2O is enriched through metasomatism compared with normal depleted mantle and primitive mantle, in trace-element patterns it shows a negative anomaly relative to neighbouring elements (for example, Fig. 2). The high $^{187}Re/^{188}Os$ and $^{187}Os/^{188}Os$ ratios in these harzburgites show that carbonatite metasomatism enriches the SCLM with high Re/Os; with time, this results in high $^{187}Os/^{188}Os$ (discussed further in Supplementary Information (see the Os evolution model) and Extended Data Fig. 5). Samples not specified as lherzolite or harzburgite in the original references are not included.

Os evolution model) illustrates that SCLM that formed in the late Archean–early Proterozoic and underwent carbonatite metasomatism can evolve $^{187}Os/^{188}Os$ ratios that are much higher than HIMU lavas; moreover, the 80:20 mixture of normal melt-depleted lherzolite and metasomatized harzburgite used to model the trace elements (Fig. 2) can reproduce the observed HIMU $^{187}Os/^{188}Os$ ratios of around 0.15 (Extended Data Fig. 5). These observations are consistent with the high $^{187}Os/^{188}Os$ ratios observed in kimberlites, which vary between 0.21 and 0.28 (ref. 28). Thus, we conclude that high Os isotope ratios are likely to develop in Archean to early Proterozoic carbonatite-metasomatized peridotite in the SCLM, confirming that it is a viable source for HIMU magmas.

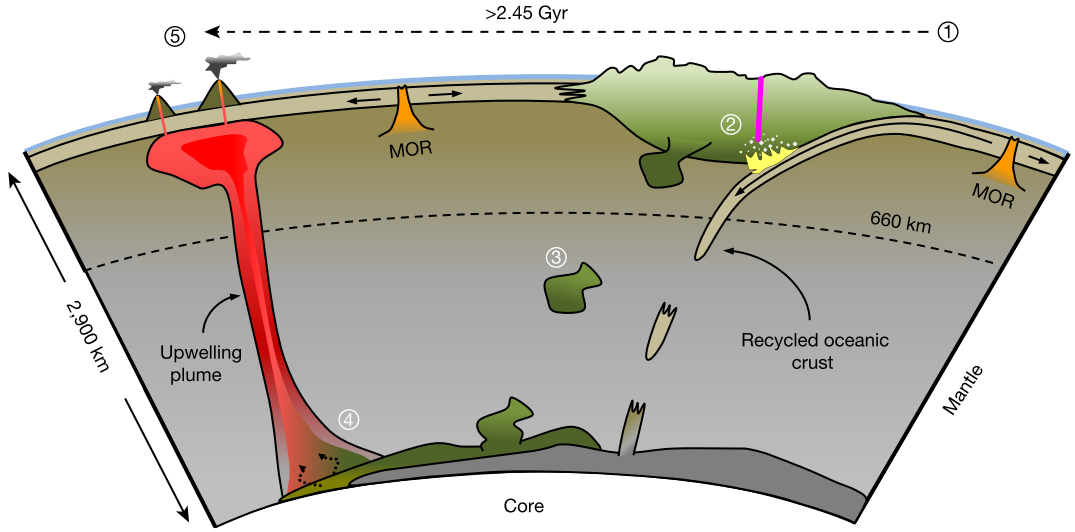

Figure 4 | Conceptual model for the evolution of the HIMU mantle source. (1) Subduction during the Archean or early Proterozoic recycled incompatible elements and mass-independent fractionated sulfur[8] from the Earth's surface to the mantle. (2) The subducting slab released fluids-melts with carbonatitic affinity that metasomatized the (melt-depleted) SCLM and also produced diamonds (white diamonds), and are related to kimberlite eruption (purple line); metasomatized SCLM develops high Pb and Os isotope ratios with time. (3) The SCLM delaminated and was transported to a mantle boundary layer, probably the core–mantle boundary. (4) Entrainment of recycled SCLM into upwelling plume at the core–mantle boundary. (5) The upwelling plume generated the HIMU OIB.

Our new evidence points to peridotitic, carbonatite-metasomatized SCLM as the source of the distinct trace-element and isotopic signatures of the HIMU mantle end-member. That this metasomatism is a consequence of Archean–early Proterozoic subduction is indicated by sulfur inclusions in HIMU lavas that show mass-independent isotope fractionation signatures[8]. Subduction of Archean carbonate, characterized by low Sr isotope ratios that are similar to present-day OIBs[29] is also consistent with the low Sr isotope ratios of HIMU basalts (Extended Data Fig. 1). Further evidence that Archean surface material is stored in the SCLM is provided by the mass-independent fractionated sulfur signatures in diamonds sampled by Phanerozoic kimberlites[30]. To become an OIB source, the metasomatized SCLM had to be incorporated into the convecting mantle and transported to a mantle boundary layer, probably the core–mantle boundary, where it eventually became part of upwelling mantle plumes (Fig. 4). Because transport of SCLM material in bulk to the convecting mantle would not fractionate parent/daughter elements, the isotopic evolution of HIMU lavas and the timing of this important event remain unconstrained. Nevertheless, the connection between HIMU lavas and SCLM carbonatite metasomatism provides strong evidence for the cycling of old continental roots into the convecting mantle, which sometimes becomes OIB. Over thirty years ago, McKenzie and O'Nions[31] proposed that delamination of SCLM followed by storage in a boundary layer is a major process in OIB formation, and this was followed by the identification of the HIMU–EM1 LoNd mantle array by Hart *et al.*[25] and their suggestion that it is derived from delaminated SCLM[25]. However, these ideas have not been generally accepted. It was also proposed that the HIMU end-member was metasomatically produced[25,32]. Our findings confirm that the SCLM plays a major role in forming HIMU OIBs and provide new support for the hypothesis[25] that the entire LoNd mantle array may be derived from delaminated SCLM.

Online Content Methods, along with any additional Extended Data display items and Source Data, are available in the online version of the paper; references unique to these sections appear only in the online paper.

Received 8 December 2015; accepted 11 July 2016.
Published online 5 September; corrected online 28 September 2016 (see full-text HTML version for details).

1. Zindler, A. & Hart, S. Chemical geodynamics. *Annu. Rev. Earth Planet. Sci.* **14,** 493–571 (1986).
2. Zindler, A., Jagoutz, E. & Goldstein, S. Nd, Sr and Pb isotopic systematics in a three-component mantle: a new perspective. *Nature* **298,** 519–523 (1982).
3. Chauvel, C., Hofmann, A. W. & Vidal, P. HIMU-EM – the French Polynesian connection. *Earth Planet. Sci. Lett.* **110,** 99–119 (1992).
4. Hofmann, A. W. Mantle geochemistry: the message from oceanic volcanism. *Nature* **385,** 219–229 (1997).
5. Hanyu, T. *et al.* Geochemical characteristics and origin of the HIMU reservoir: a possible mantle plume source in the lower mantle. *Geochem. Geophys. Geosyst.* **12,** Q0AC09 (2011).
6. Herzberg, C. *et al.* Phantom Archean crust in Mangaia hotspot lavas and the meaning of heterogeneous mantle. *Earth Planet. Sci. Lett.* **396,** 97–106 (2014).
7. Weiss, Y., Griffin, W. L., Bell, D. R. & Navon, O. High-Mg carbonatitic melts in diamonds, kimberlites and the sub-continental lithosphere. *Earth Planet. Sci. Lett.* **309,** 337–347 (2011).
8. Cabral, R. A. *et al.* Anomalous sulphur isotopes in plume lavas reveal deep mantle storage of Archaean crust. *Nature* **496,** 490–493 (2013).
9. Hauri, E. H. & Hart, S. R. ReOs isotope systematics of HIMU and EMII oceanic island basalts from the south Pacific Ocean. *Earth Planet. Sci. Lett.* **114,** 353–371 (1993).
10. Stracke, A. Earth's heterogeneous mantle: a product of convection-driven interaction between crust and mantle. *Chem. Geol.* **330–331,** 274–299 (2012).
11. Class, C., Goldstein, S. L., Altherr, R. & Bachelery, P. The process of plume–lithosphere interactions in the ocean basins: the case of Grande Comore. *J. Petrol.* **39,** 881–903 (1998).
12. Sobolev, A. V. *et al.* The amount of recycled crust in sources of mantle-derived melts. *Science* **316,** 412–417 (2007).
13. Matzen, A. K., Baker, M. B., Beckett, J. R. & Stolper, E. M. The temperature and pressure dependence of nickel partitioning between olivine and silicate melt. *J. Petrol.* **54,** 2521–2545 (2013).
14. Balta, J. B., Asimow, P. D. & Mosenfelder, J. L. Manganese partitioning during hydrous melting of peridotite. *Geochim. Cosmochim. Acta* **75,** 5819–5833 (2011).
15. De Hoog, J. C. M., Gall, L. & Cornell, D. H. Trace-element geochemistry of mantle olivine and application to mantle petrogenesis and geothermobarometry. *Chem. Geol.* **270,** 196–215 (2010).
16. Coogan, L. A., Saunders, A. D. & Wilson, R. N. Aluminum-in-olivine thermometry of primitive basalts: evidence of an anomalously hot mantle source for large igneous provinces. *Chem. Geol.* **368,** 1–10 (2014).
17. Agee, C. B. & Walker, D. Aluminum partitioning between olivine and ultrabasic silicate liquid to 6 GPa. *Contrib. Mineral. Petrol.* **105,** 243–254 (1990).
18. Saal, A. E., Hart, S. R., Shimizu, N., Hauri, E. H. & Layne, G. D. Pb isotopic variability in melt inclusions from oceanic island basalts, Polynesia. *Science* **282,** 1481–1484 (1998).
19. Jackson, M. G. & Dasgupta, R. Compositions of HIMU, EM1, and EM2 from global trends between radiogenic isotopes and major elements in ocean island basalts. *Earth Planet. Sci. Lett.* **276,** 175–186 (2008).
20. Castillo, P. R. The recycling of marine carbonates and sources of HIMU and FOZO ocean island basalts. *Lithos* **216–217,** 254–263 (2015).
21. Willbold, M. & Stracke, A. Trace element composition of mantle end-members: Implications for recycling of oceanic and upper and lower continental crust. *Geochem. Geophys. Geosyst.* **7,** Q04004 (2006).
22. Becker, M. & Le Roex, A. P. Geochemistry of South African on- and off-craton, Group I and Group II kimberlites: petrogenesis and source region evolution. *J. Petrol.* **47,** 673–703 (2006).
23. Gregoire, M., Bell, D. R. & Le Roex, A. P. Garnet lherzolites from the Kaapvaal craton (South Africa): trace element evidence for a metasomatic history. *J. Petrol.* **44,** 629–657 (2003).
24. McDonough, W. F. Contraints on the composition of the continental lithospheric mantle. *Earth Planet. Sci. Lett.* **101,** 1–18 (1990).
25. Hart, S. R., Gerlach, D. C. & White, W. M. A possible new Sr–Nd–Pb mantle array and consequences for mantle mixing. *Geochim. Cosmochim. Acta* **50,** 1551–1557 (1986).
26. Shirey, S. B. & Walker, R. J. The Re-Os isotope system in cosmochemistry and high-temperature geochemistry. *Annu. Rev. Earth Planet. Sci.* **26,** 423–500 (1998).
27. Rudnick, R. L., McDonough, W. F. & Chappell, B. W. Carbonatite metasomatism in the northern Tanzanian mantle: petrographic and geochemical characteristics. *Earth Planet. Sci. Lett.* **114,** 463–475 (1993).
28. Graham, S., Lambert, D. & Shee, S. The petrogenesis of carbonatite, melnoite and kimberlite from the Eastern Goldfields Province, Yilgarn Craton. *Lithos* **76,** 519–533 (2004).
29. Veizer, J. & Compston, W. 87Sr/86Sr in Precambrian carbonates as an index of crustal evolution. *Geochim. Cosmochim. Acta* **40,** 905–914 (1976).
30. Farquhar, J. *et al.* Mass-independent sulfur of inclusions in diamond and sulfur recycling on early earth. *Science* **298,** 2369–2372 (2002).
31. McKenzie, D. & O'Nions, R. K. Mantle reservoirs and ocean island basalts. *Nature* **301,** 229–231 (1983).
32. Stein, M., Navon, O. & Kessel, R. Chromatographic metasomatism of the Arabian–Nubian lithosphere. *Earth Planet. Sci. Lett.* **152,** 75–91 (1997).

Supplementary Information is available in the online version of the paper.

Acknowledgements We thank S. Lambart, D. G. Pearson, S. Aulbach and D. Walker for discussions, A. W. Hofmann for discussions and an informal review, J. Gross and B. A. Goldoff for help with the EPMA analyses, and K. Lehnert and A. Johansson for help with accessing the xenolith data in EarthChem's PetDB database. This work was supported by an LDEO Postdoctoral Fellowship for Y.W., NSF grant EAR13-48045 to Y.W., C.C. and S.L.G., and the Storke Endowment of the Columbia University Department of Earth and Environmental Sciences. This is Lamont–Doherty Earth Observatory contribution number 8046.

Author Contributions Y.W., C.C. and S.L.G. conceived the project, developed the model and wrote the paper. Y.W. preformed the EPMA analyses. T.H. provided the olivine samples for the study and contributed to the paper.

Author Information The new data (Supplementary Data 1, http://dx.doi.org/10.1594/IEDA/100601) as well as the compiled xenolith data set used here (Supplementary Data 2, http://dx.doi.org/10.1594/IEDA/100602) have been submitted to the EarthChem Library (http://www.earthchem.org/library). Reprints and permissions information is available at www.nature.com/reprints. The authors declare no competing financial interests. Readers are welcome to comment on the online version of the paper. Correspondence and requests for materials should be addressed to Y.W. (yweiss@ldeo.columbia.edu), S.L.G. (steveg@ldeo.columbia.edu), C.C. (class@ldeo.columbia.edu) and T.H. (hanyut@jamstec.go.jp).

Reviewer Information *Nature* thanks E. Hauri and W. White for their contribution to the peer review of this work.

METHODS

Samples and analytical methods. Olivine phenocrysts were selected from Mangaia, Tubuai and Karthala lavas (five samples from each volcano) that were previously analysed for their major and trace elements and Sr, Nd, Pb, Os and He isotopic compositions[5,11,33–35].

Electron probe microanalyser (EPMA) analyses. The phenocrysts were mounted in epoxy, polished to 0.1 μm, cleaned ultrasonically in ethanol and distilled water and finally carbon coated. They were then analysed for major (Si, Mg and Fe) and minor elements (Ca, Ni, Cr, Mn and Al) using a Cameca SX100, equipped with five wavelength dispersive spectrometers at The American Museum of Natural History (AMNH), New York. The electron beam size was 1 μm, with an acceleration voltage of 15 kV and a current of 120 nA during all analyses. Peak counting was 30 s for the major elements (Si, Mg and Fe) and 180 s for minor elements (Ca, Ni, Cr, Mn and Al); background counting was half-time peak counting on each background position. A set of reference materials were used for calibration. San-Carlos olivine (NMNH# 111312-44) was used to calibrate Si, Mg and Fe, Wakefield Diopside for Ca, chromite ($MgCr_2O_4$) for Cr, rhodonite ($MnSiO_3$) for Mn, spinel ($MgAl_2O_4$) for Al and Ni-diopside glass (synthetic) for Ni. These standards were repeatedly analysed as unknowns approximately every 30 analyses for calibration control and to monitor instrument stability. The $\pm 2\sigma$ analytical uncertainty in 206 analyses of San Carlos olivine gave ±0.12 mol% Fo, ±70 p.p.m. Ni, ±66 p.p.m. Ca, ±59 p.p.m. Mn, ±28 p.p.m. Al and ±23 p.p.m. Cr. Full analyses of Mangaia, Tubuai and Karthala olivines and the San Carlos olivine (NMNH# 111312-44) standard are in Supplementary Data 1.

33. Class, C., Goldstein, S. L. & Shirey, S. B. Osmium isotopes in Grande Comore lavas: a new extreme among a spectrum of EM-type mantle endmembers. *Earth Planet. Sci. Lett.* **284,** 219–227 (2009).
34. Class, C., Goldstein, S. L., Stute, M., Kurz, M. D. & Schlosser, P. Grand Comore Island: a well-constrained "low He-3/He-4" mantle plume. *Earth Planet. Sci. Lett.* **233,** 391–409 (2005).
35. Hanyu, T., Tatsumi, Y. & Kimura, J.-I. Constraints on the origin of the HIMU reservoir from He–Ne–Ar isotope systematics. *Earth Planet. Sci. Lett.* **307,** 377–386 (2011).
36. Kramers, J. D. Lead and strontium isotopes in Cretaceous kimberlites and mantle-derived xenoliths from Southern Africa. *Earth Planet. Sci. Lett.* **34,** 419–431 (1977).
37. Collerson, K. D., Williams, Q., Ewart, A. E. & Murphy, D. T. Origin of HIMU and EM-1 domains sampled by ocean island basalts, kimberlites and carbonatites: the role of CO2-fluxed lower mantle melting in thermochemical upwellings. *Phys. Earth Planet. Inter.* **181,** 112–131 (2010).
38. Tilton, G. R. & Bell, K. Sr–Nd–Pb isotope relationships in Late Archean carbonatites and alkaline complexes: applications to the geochemical evolution of Archean mantle. *Geochim. Cosmochim. Acta* **58,** 3145–3154 (1994).
39. Bell, K. & Tilton, G. R. Nd, Pb and Sr isotopic compositions of East African carbonatites: evidence for mantle mixing and plume inhomogeneity. *J. Petrol.* **42,** 1927–1945 (2001).
40. Bizimis, M., Salters, V. J. M. & Dawson, J. B. The brevity of carbonatite sources in the mantle: evidence from Hf isotopes. *Contrib. Mineral. Petrol.* **145,** 281–300 (2003).
41. McNutt, M. K. Marine geodynamics: depth-age revisited. *Rev. Geophys.* **33,** 413–418 (1995).
42. Braun, M. G. & Kelemen, P. B. Dunite distribution in the Oman ophiolite: implications for melt flux through porous dunite conduits. *Geochem. Geophys. Geosyst.* **3,** 8603 (2002).
43. Herzberg, C. & Asimow, P. D. Petrology of some oceanic island basalts: PRIMELT2.XLS software for primary magma calculation. *Geochem. Geophys. Geosyst.* **9,** Q09001 (2008).
44. Korenaga, J. & Kelemen, P. B. Major element heterogeneity in the mantle source of the North Atlantic igneous province. *Earth Planet. Sci. Lett.* **184,** 251–268 (2000).

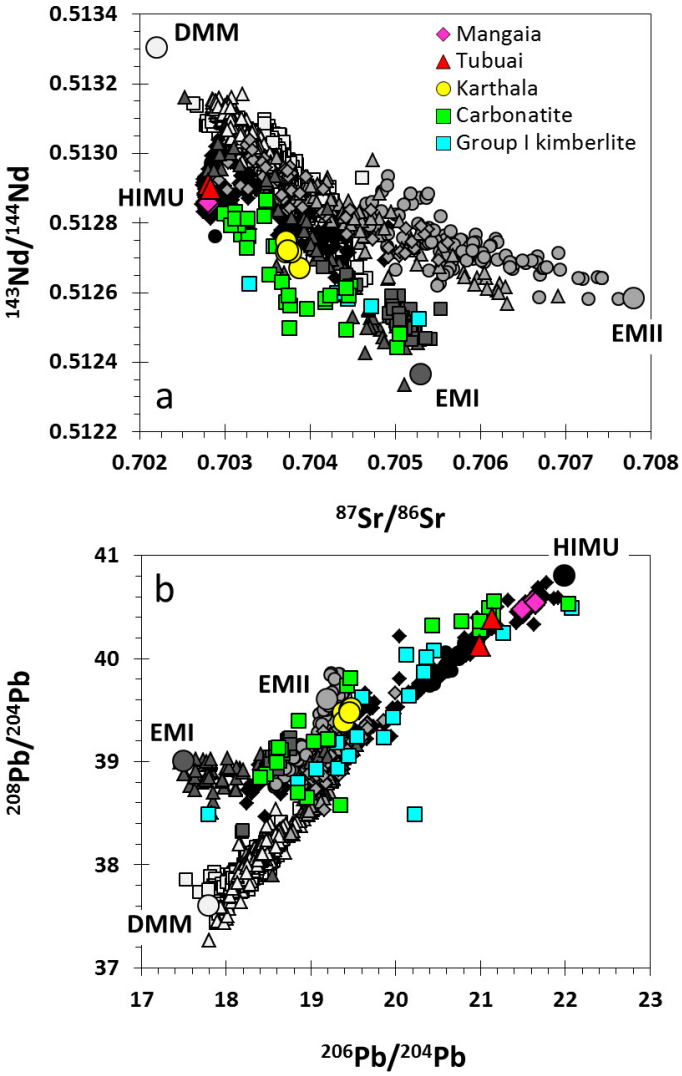

Extended Data Figure 1 | Sr–Nd–Pb isotopes of Mangaia, Tubuai and Karthala samples in this study, African Group I kimberlites and continental carbonatites. a, $^{143}Nd/^{144}Nd$ versus $^{87}Sr/^{86}Sr$. **b,** $^{208}Pb/^{204}Pb$ versus $^{206}Pb/^{204}Pb$. The data illustrate the compositional range between the global mantle endmembers (DMM, depleted MORB mantle; EM1; EM2 and HIMU); mixing on this diagram is linear. Data sources: Mangaia and Tubuai (ref. 5), Karthala (ref. 11), kimberlites (refs 22, 36, 37) and continental carbonatites (refs 38–40). The mantle end-member components are from ref. 1; the grey and black data points are from Hawaii, Iceland, St Helena, Cook–Austral Islands, Samoa, Society, Marquesas, Pitcairn and Tristan (from the compilation of ref. 10).

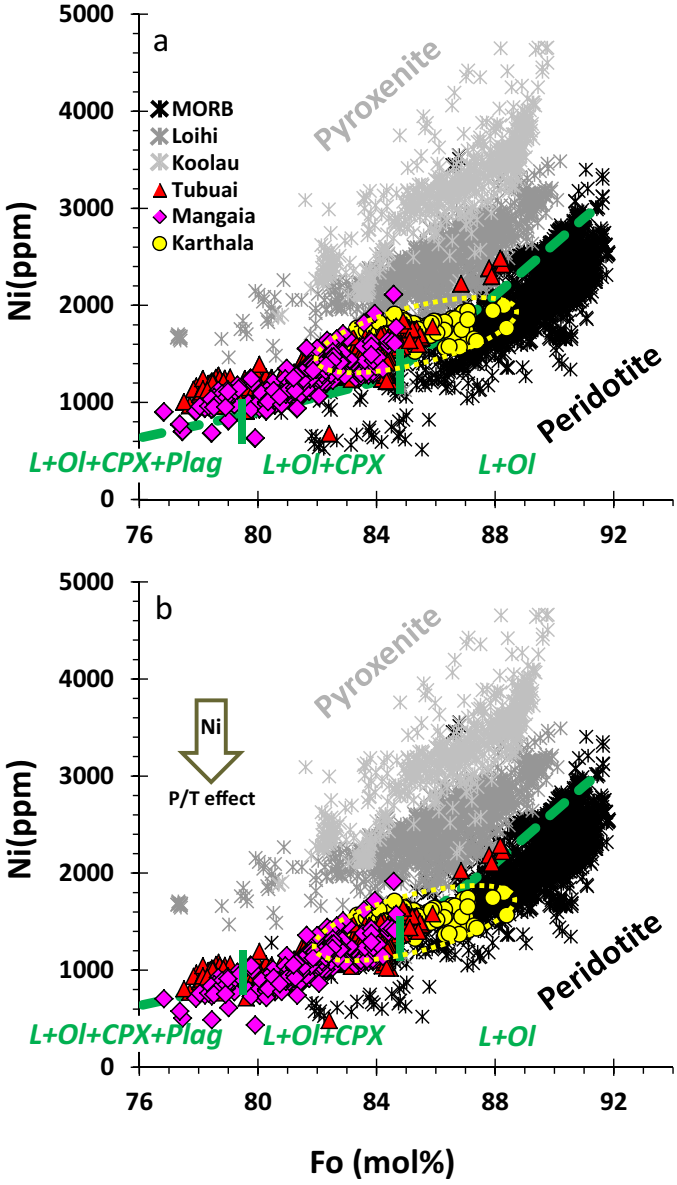

Extended Data Figure 2 | Pressure–temperature corrections to the Ni contents of Mangaia, Tubuai and Karthala olivine phenocrysts. **a**, 300 p.p.m. Ni. **b**, 500 p.p.m. Ni. Following ref. 13, we calculated Ni in near-surface olivine in equilibrium with Mangaia and Karthala primary magmas at different segregation pressures (ΔT in the model). On the basis of the age of the oceanic crust of Mangaia and Tubuai (80–120 Ma) and Karthala (approximately 140 Ma), which are equivalent to estimated lithosphere thicknesses of around 75–100 km (ref. 41), we assume that the difference between the pressures (P) of segregation of these lavas compared to MORBs (around 1 GPa; ref. 42) is 1.25–2.00 GPa, equivalent to $\Delta T = 70$–110 °C. This difference in the segregation pressures corresponds to 300–500 p.p.m. Ni (the arrow pointing to lower Ni indicates the effect of increasing pressure and/or temperature ('P/T effect') on Ni-in-olivine). When corrected, Mangaia, Tubuai and Karthala data agree with the modelled olivine liquid line of descent for Mangaia primary magmas[6] (that is, the green dashed line; L, liquid; Ol, olivine; Cpx, clinopyroxene; Plag, plagioclase), and lie on an extension of the crystallization trend of MORB phenocryst compositions. These relationships support the connection between the olivine phenocryst compositions and a peridotite source lithology. For the calculations, we used PRIMELT2 (ref. 43) to determine the parental magma compositions, the Fo content of the olivine in equilibrium with this liquid and the liquidus temperature at 1 bar; and Ni = 0.37 wt% for the residual peridotite olivine, which is the mean global value for olivines from spinel and garnet peridotites[44]. The yellow ellipses encompass >95% of the data points for Karthala olivine (see Supplementary Data 1).

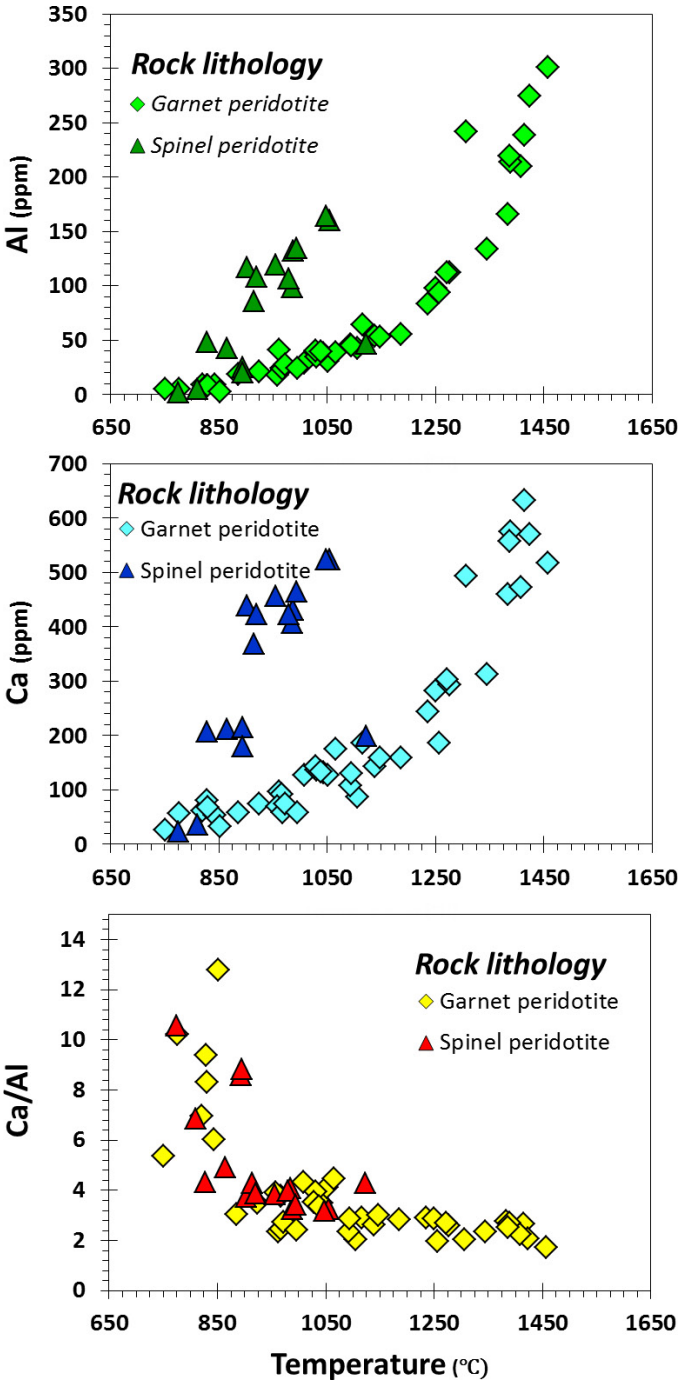

Extended Data Figure 3 | Ca and Al in olivine from garnet and spinel peridotite xenoliths as a function of temperature. Top, Al concentration. Middle, Ca concentration. Bottom, Ca/Al ratio. Xenolith data and temperatures are from ref. 15. The data show that while partitioning of both Ca and Al into olivine increase with temperature, the Ca/Al ratios in olivine initially decrease and become nearly constant with increasing temperature.

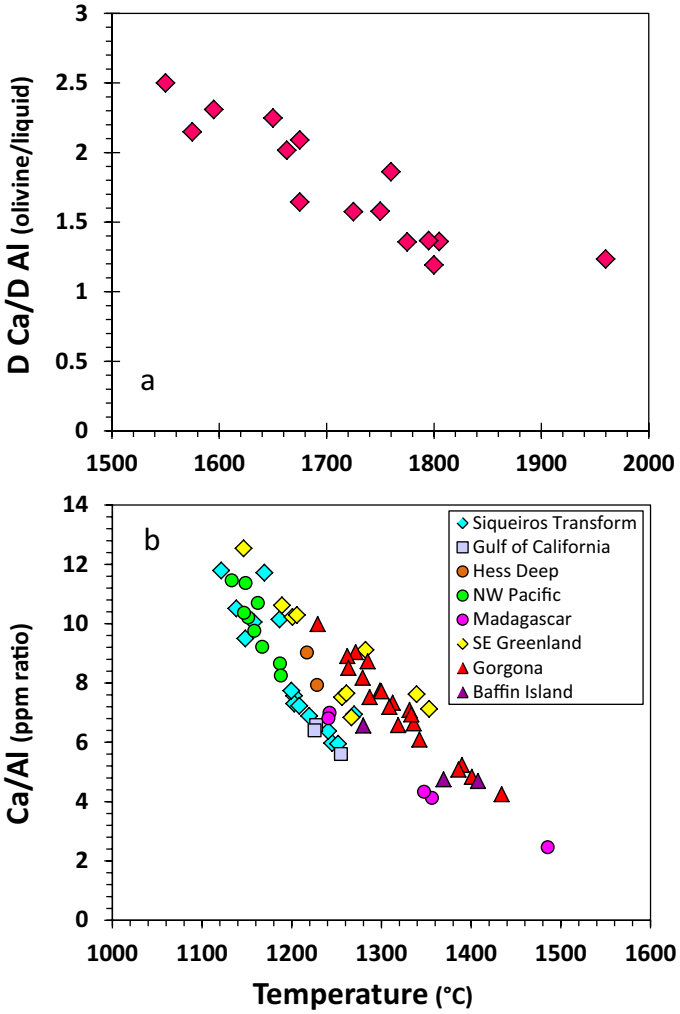

Extended Data Figure 4 | Ca and Al partitioning with temperature in olivines in basalts. a, Ratio of Ca and Al partition coefficients (*D*). **b**, Ca/Al ratios in olivine phenocrysts. The experimentally determined *D* values for Ca- and Al-in-olivine, in equilibrium with a peridotite-derived melt, are from ref. 17; they were determined for increasing temperature and pressure. Data for Ca and Al in olivine phenocrysts from MORB (NW Pacific, Hess Deep, Gulf of California, Siqueiros Transform) and large igneous provinces (LIPs; SE Greenland, Baffin Island, Gorgona, Madagascar) are from ref. 16; temperatures were determined on the basis of the Al-in-olivine thermometer[16]. Both the experimental results and the measured Ca and Al contents in crystallizing olivines show decreasing Ca/Al ratios with increasing temperature. On the basis of these data and the observations in Extended Data Fig. 3, Ca/Al ratios in olivine phenocrysts from magmatic systems can be expected to decrease with increasing temperature. In contrast, our data from HIMU hot plumes show very high Ca/Al ratios in olivine phenocrysts compared with low Ca/Al ratios in phenocrysts from cooler MORB lavas (or other hot OIBs) (see Fig. 1). Temperature differences therefore cannot explain the Ca/Al variations in olivine from OIB and MORB lavas. We thus conclude that the high Ca/Al ratios of HIMU olivine phenocrysts and lavas instead reflect the compositions of the HIMU magma source.

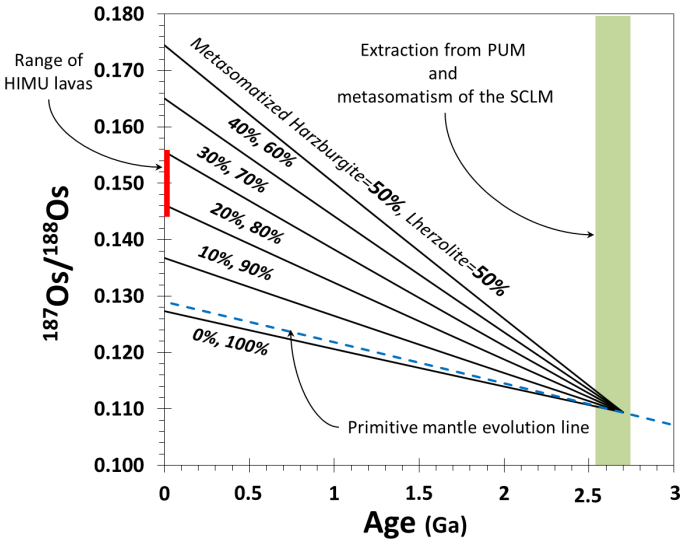

Extended Data Figure 5 | $^{187}Os/^{188}Os$ evolution of mixtures of lherzolite and metasomatized harzburgite. The metasomatic event in the SCLM took place in the Archean or early Proterozoic and involved materials that had been at the Earth's surface (on the basis of the observation that HIMU lavas contain sulfur that shows mass-independent fractionation)[8]. We use 2.7 Ga for this example. Our study determined that the metasomatizing agent is subduction-derived carbonatitic fluids/melts. The primitive upper mantle (PUM) evolution line is based on present-day values of $^{187}Os/^{188}Os = 0.129$ and $^{187}Re/^{188}Os = 0.43$ (ref. 26); at 2.7 Ga the $^{187}Os/^{188}Os$ of PUM was 0.109. The figure shows evolution lines from the PUM at 2.7 Ga for mixtures of lherzolite and metasomatized harzburgite ranging from 50% to 100% lherzolite. The Re/Os ratios of the normal (lherzolite) and metasomatized (harzburgitic) SCLM are from the averages of 143 cratonic lherzolite xenoliths ($^{187}Re/^{188}Os = 0.4$) and 31 harzburgite xenoliths ($^{187}Re/^{188}Os = 2.44$), respectively, all with Mg# between 0.910 and 0.935 from the mantle xenolith database in PetDB (see Supplementary Data 2). For a metasomatic event at 2.7 Ga, only 18%–30% metasomatized harzburgite is required to reproduce the $^{187}Os/^{188}Os$ ratios of HIMU lavas.